Dynamic dipole polarizabilities for the low-lying triplet states of helium

Yong-Hui Zhang,[1,2] Li-Yan Tang,[2,*] Xian-Zhou Zhang,[1,†] and Ting-Yun Shi[2,3]

[1]*Department of Physics, Henan Normal University, XinXiang 453007, People's Republic of China*

[2]*State Key Laboratory of Magnetic Resonance and Atomic and Molecular Physics, Wuhan Institute of Physics and Mathematics, Chinese Academy of Sciences, Wuhan 430071, People's Republic of China*

[3]*Center for Cold Atom Physics, Chinese Academy of Sciences, Wuhan 430071, People's Republic of China*

(Received 25 March 2015; published 24 July 2015)

The dynamic dipole polarizabilities for the four lowest triplet states ($2\,^3S$, $3\,^3S$, $2\,^3P$, and $3\,^3P$) of helium are calculated using the B-spline configuration interaction method. Present values of the static dipole polarizabilities in the length, velocity, and acceleration gauges are in good agreement with the best Hylleraas results. Also the tune-out wavelengths in the range 400 nm–4.2 μm for the four lowest triplet states are identified, and the magic wavelengths in the range 460 nm–3.5 μm for the $2\,^3S \rightarrow 3\,^3S$, $2\,^3S \rightarrow 2\,^3P$, and $2\,^3S \rightarrow 3\,^3P$ transitions are determined. We show that the tune-out wavelength of $2\,^3S$ state is 413.038 28(3) nm, which corroborates the value of Mitroy and Tang [Phys. Rev. A **88**, 052515 (2013)], and the magic wavelength around 1066 nm for the $2\,^3S \rightarrow 3\,^3P$ transition can be expected for precision measurement to determine the ratio of transition matrix elements $(2\,^3S \rightarrow 2\,^3P)/(3\,^3P \rightarrow 6\,^3S)$.

DOI: 10.1103/PhysRevA.92.012515 PACS number(s): 31.15.ap, 31.15.ac, 32.10.Dk

I. INTRODUCTION

Precise calculations of dynamic dipole polarizabilities for atoms are of interest due to their importance in a number of applications. First, dynamic dipole polarizabilities can be used directly to analyze the ac Stark shift to pursue higher-precision atomic clocks [1,2]. Second, investigation of the dynamic dipole polarizabilities can derive the magic wavelengths and tune-out wavelengths, which open a new route to determine the line strength ratio [2,3] and to test the relativistic and quantum electrodynamic (QED) effects upon the transition matrix element not on the energy [4,5]. And third, since both the trapping potential depth and the photon-scattering rate are dependent on the polarizabilities, the calculations of the dynamic dipole polarizabilities can provide reliable reference for experimental design to trap atoms in efficiency [6,7].

As the simplest two-electron system, the accurate theoretical calculations and experimental measurements of the energy levels for helium can be used to test the the three-body bound QED theory [8,9], to determine the fine-structure constant with high precision [10–12], to extract the nuclear information without resorting to any model [13,14], and to develop the multielectron atomic structure theory [9,15]. Recently, the resonance transition $2\,^3S \rightarrow 2\,^3P$ and the doubly forbidden transition $2\,^3S \rightarrow 2\,^1S$ of helium isotopes have attracted great interest for the determination of nuclear charge radius difference [7,13,14,16]. Combining the laser cooling with magneto-optical trap techniques, the transitions $2\,^3S \rightarrow 2\,^3P$ and $2\,^3S \rightarrow 3\,^3P$ of helium are also demonstrated to produce high density quantum gas [17]. The key point to improve the experimental measurement precision for helium is to set the laser frequency at the magic wavelength to eliminate effectively the ac Stark shift induced by the trap light.

At present, there are many literatures focusing on the accurate calculations of the energy and polarizabilities [18–24] for the ground state of helium. For example, the nonrelativistic ground-state energy has been achieved up to 46 digits [25], and the static dipole polarizability of the ground-state helium, which includes the effect of mass polarization, the relativistic and leading QED corrections, has been determined to 1.383 191(2) within 2 ppm accuracy [26]. However, compared with the ground state, there are several calculations of dynamic polarizabilities for the triplet states of helium. For the metastable state $2\,^3S$ of helium, Glover *et al.* listed the rigorous upper and lower bounds of the dynamic dipole polarizabilities [27]. Chung provided dynamic polarizabilities for frequencies up to the second excitation threshold by using a variation-perturbation scheme [28]. Chen used a configuration interaction (CI) scheme with B-spline functions [29] to improve the convergence of the dynamic dipole polarizabilities [30,31]. And Rérat *et al.* presented the dynamic dipole polarizabilities of helium at both real and imaginary frequencies using the time-dependent gauge-invariant method [32]. In 2005, Chernov *et al.* calculated the dynamic polarizabilities [33] by using the quantum defect Green-function formalism. For other triplet states of helium, there are few reports which can be referenced [33,34].

In this work, we perform the calculations of static dipole polarizabilities for the low-lying triplet states $2\,^3S$, $2\,^3P$, $3\,^3S$, and $3\,^3P$ of helium with the configuration interaction method based on B-spline basis set in the length, velocity, and acceleration gauges. Then the dynamic dipole polarizabilities of $2\,^3S$, $2\,^3P$ for frequencies below the second excitation threshold and $3\,^3S$, $3\,^3P$ for frequencies below the first ionization threshold are calculated utilizing oscillator strengths and energy differences obtained in the length gauge. In addition, using the dynamic dipole polarizabilities, the magic wavelengths for the three transitions $2\,^3S \rightarrow 3\,^3S$, $2\,^3S \rightarrow 2\,^3P$, and $2\,^3S \rightarrow 3\,^3P$, and the tune-out wavelengths for the four lowest triplet states $2\,^3S$, $2\,^3P$, $3\,^3S$, and $3\,^3P$ are determined with high accuracy. The atomic units are used throughout this paper unless specifically mentioned.

*lytang@wipm.ac.cn

†xz-zhang@henannu.edu.cn

 ©2015 American Physical Society

II. DIPOLE POLARIZABILITY

The dynamic dipole polarizability for the magnetic sublevel $|L_g M_g\rangle$ is

$$\alpha_{L_g M_g}(\omega) = \alpha_1(\omega) + \frac{3M_g^2 - L_g(L_g+1)}{L_g(2L_g-1)}\alpha_1^T(\omega), \tag{1}$$

where $\alpha_1(\omega)$ and $\alpha_1^T(\omega)$ are the dynamic scalar and tensor dipole polarizabilities respectively; they can be expressed as the summation of all allowed-transition intermediate states, including the continuum,

$$\alpha_1(\omega) = \sum_{n\neq g} \frac{f_{gn}^{(1)}}{(\Delta E_{gn})^2 - \omega^2}, \tag{2}$$

$$\alpha_1^T(\omega) = \sum_{n\neq g}(-1)^{L_g+L_n}\sqrt{\frac{30(2L_g+1)L_g(2L_g-1)}{(2L_g+3)(L_g+1)}}\begin{Bmatrix} 1 & 1 & 2 \\ L_g & L_g & L_n \end{Bmatrix}\frac{f_{gn}^{(1)}}{(\Delta E_{gn})^2 - \omega^2}, \tag{3}$$

where ΔE_{gn} is the transition energy between the initial state $|N_g L_g M_g\rangle$ and the intermediate state $|N_n L_n M_n\rangle$, ω is the photon energy of external electric field, and the dipole oscillator strength f_{gn} have different expressions in the length (L), velocity (V), and acceleration (A) gauges respectively,

$$f_{gn}^{(L)} = \frac{2|\langle N_g L_g \| \sum_{i=1,2} r_i C^{(1)}(\hat{r}_i) \| N_n L_n\rangle|^2 \Delta E_{gn}}{3(2L_g+1)}, \tag{4}$$

$$f_{gn}^{(V)} = \frac{2|\langle N_g L_g \| \sum_{i=1,2} \frac{d}{dr_i} C^{(1)}(\hat{r}_i) + b(\ell_k;\ell_\ell) r_i^{-1} C^{(1)}(\hat{r}_i) \| N_n L_n\rangle|^2 (\Delta E_{gn})^{-1}}{3(2L_g+1)}, \tag{5}$$

$$f_{gn}^{(A)} = \frac{2|\langle N_g L_g \| \sum_{i=1,2} Z r_i^{-2} C^{(1)}(\hat{r}_i) \| N_n L_n\rangle|^2 (\Delta E_{gn})^{-3}}{3(2L_g+1)}, \tag{6}$$

where $\sum_{i=1,2} r_i C^{(1)}(\hat{r}_i)$ is the electronic dipole transition operator of the two-electron system, Z is the nuclear charge number, ℓ_k or ℓ_ℓ are the orbital quantum number of a electron, and the function $b(\ell;\lambda)$ is defined as

$$\begin{cases} b(\ell;\ell-1) = \ell+1, \\ b(\ell;\ell+1) = -\ell. \end{cases} \tag{7}$$

According to the Eqs. (2) and (3), for the case of $L_g = 0$ initial state, the dynamic scalar and tensor dipole polarizabilities are

$$\alpha_1(\omega) = \alpha_1(P,\omega), \tag{8}$$

$$\alpha_1^T(\omega) = 0, \tag{9}$$

where $\alpha_1(P,\omega)$ represents the contributions of the intermediate state with the angular momentum number $L_n = 1$.

For the initial state of $L_g = 1$, the dynamic scalar and tensor dipole polarizabilities are expressed as

$$\alpha_1(\omega) = \alpha_1(S,\omega) + \alpha_1(P,\omega) + \alpha_1(D,\omega), \tag{10}$$

$$\alpha_1^T(\omega) = -\alpha_1(S,\omega) + \tfrac{1}{2}\alpha_1(P,\omega) - \tfrac{1}{10}\alpha_1(D,\omega), \tag{11}$$

where $\alpha_1(S,\omega)$ and $\alpha_1(D,\omega)$ are the contributions of the natural parity state $(ss)S$ and $(sd)D$ respectively, and $\alpha_1(P,\omega)$ is the contribution from the unnatural parity state of $(pp')P$ electron configuration.

In order to calculate the dynamic dipole polarizabilities, the fundamental atomic structure information of energies and wave functions need to be obtained first. In our calculations, the configuration interaction method based on B-spline functions are adopted to get the energies and wave functions for helium.

III. CONFIGURATION INTERACTION WITH B-SPLINE FUNCTION

The Hamiltonian for the two-electron system is given in second-quantized form as

$$H = \sum_i \varepsilon_i a_i^\dagger a_i + \frac{1}{2}\sum_{ijk\ell} g_{ijk\ell} a_i^\dagger a_j^\dagger a_\ell a_k, \tag{12}$$

where ε_i is the ith energy eigenvalue of the single-particle Schrödinger equation, g_{ijkl} is the two-particle matrix element of the Coulomb interaction, and $a_i^\dagger$ and a_i are creation and annihilation operators for the ith electronic state respectively. The single-particle quantum state is presented as $|n_i \ell_i m_i m_{s_i}\rangle$, here n_i is the principal quantum number, ℓ_i is the orbital angular momentum, m_i and m_{s_i} are the orbital and spin angular momentum projection, respectively.

The two-electron wave function $\psi_{ij}(LS)$ is expressed as a linear combination of configuration-state wave functions $\phi_{ij}(LS)$,

$$\psi_{ij}(LS) = \sum_{ij} c_{ij}\phi_{ij}(LS), \tag{13}$$

and the configuration-state wave function has the following expression:

$$\phi_{ij}(LS) = \eta_{ij}\sum_{m_i m_j}\sum_{m_{s_i} m_{s_j}} \langle \ell_i m_i; \ell_j m_j | LM\rangle \times \langle 1/2 m_{s_i}; 1/2 m_{s_j} | SM_S\rangle a_i^\dagger a_j^\dagger |0\rangle, \tag{14}$$

where η_{ij} is a normalization constant given by

$$\eta_{ij} = \begin{cases} 1, & i \neq j, \\ \frac{1}{\sqrt{2}}, & i = j. \end{cases} \tag{15}$$

The Clebsch-Gordan coefficients $\langle \ell_i m_i; \ell_j m_j | LM\rangle$ and $\langle 1/2 m_{s_i}; 1/2 m_{s_j} | SM_S\rangle$ represent $\ell\ell$ and ss coupling, respectively, $|0\rangle$ is the vacuum state, and $a_i^\dagger|0\rangle$ represents the ith eigenwave function of the single-particle Schrödinger equation with energy eigenvalue ε_i. The configuration-state wave functions are independent of magnetic quantum numbers of m_i, m_j, m_{s_i}, and m_{s_j}. From the interchange symmetry of the Clebsch-Gordan coefficients, it follows that

$$\phi_{ji}(LM) = (-1)^{\ell_i+\ell_j+L+S}\phi_{ij}(LM), \tag{16}$$

which implies $\phi_{ii}(LM) = 0$ unless $L+S$ is even.

According to the expansion of the wave functions, the matrix elements of Hamiltonian are

$$\langle \psi_{ij}(LM)|H|\psi_{k\ell}(LM)\rangle = \sum_{k\ell}(\varepsilon_i+\varepsilon_j)c_{ij}c_{k\ell}\delta_{ik}\delta_{j\ell} + \sum_{ij,k\ell} V_{ij,k\ell}c_{ij}c_{k\ell}, \tag{17}$$

where the potential-energy matrix element $V_{ij,k\ell}$ between different configurations is

$$V_{ijk\ell} = \eta_{ij}\eta_{kl}\left[\sum_\nu (-1)^{\ell_j-\ell_k+L+\nu}\begin{Bmatrix}\ell_i & \ell_j & L\\ \ell_\ell & \ell_k & \nu\end{Bmatrix}X_\nu(ijk\ell) + \sum_\nu (-1)^{\ell_j-\ell_k+S+\nu}\begin{Bmatrix}\ell_i & \ell_j & L\\ \ell_k & \ell_\ell & \nu\end{Bmatrix}X_\nu(ij\ell k)\right]. \tag{18}$$

The quantity $X_\nu(ijk\ell)$ in the above equation is given by

$$X_\nu(ijk\ell) = (-1)^\nu\langle \ell_i\|C^\nu\|\ell_k\rangle\langle \ell_j\|C^\nu\|\ell_\ell\rangle R_\nu(ijk\ell), \tag{19}$$

where $\langle \ell_i\|C^\nu\|\ell_k\rangle$ is angular reduced matrix element,

$$\langle \ell_i\|C^\nu\|\ell_k\rangle = (-1)^{\ell_i}\sqrt{(2\ell_i+1)(2\ell_k+1)}\begin{Bmatrix}\ell_i & \nu & \ell_k\\ 0 & 0 & 0\end{Bmatrix}. \tag{20}$$

The two-electron radial integral $R_\nu(ijk\ell)$ of the Coulomb interaction is written as

$$R_\nu(ijk\ell) = \iint r_1^2 dr_1 r_2^2 dr_2 R_i(r_1)R_k(r_1)\frac{r_<^\nu}{r_>^{\nu+1}}R_j(r_2)R_\ell(r_2), \tag{21}$$

where $r_<$ and $r_>$ are the minimum and maximum of r_1 and r_2, and $R_i(r)$ is the radial wave function of the ith single-electron orbital.

Using the variational method, the followed configuration interaction equations can be obtained:

$$\sum_{k\ell}[(\varepsilon_i+\varepsilon_j)\delta_{ik}\delta_{jl} + V_{ijkl}]c_{kl} = \lambda c_{ij}, \tag{22}$$

where λ and c_{ij} are the eigenenergy and the expansion coefficients of eigenwave function for two-electron atom, respectively.

Before solving the CI equations, the energies and wave functions for single-electron orbital are obtained first. In our calculations, B-splines are used to expand the radial wave function for the ith single-electron orbital,

$$R_i(r) = \sum_j c_j^i B_j(r), \tag{23}$$

where c_j^i are the expansion coefficients, and the following exponential knots are employed:

$$\begin{cases} t_i = 0, & i = 1,2,\ldots,k-1,\\ t_{i+k-1} = R_0\dfrac{\exp\left[\gamma R_0\left(\frac{i-1}{N-2}\right)\right]-1}{\exp[\gamma R_0]-1}, & i = 1,2,\ldots,N-1,\\ t_i = R_0, & i = N+k-1, N+k. \end{cases} \tag{24}$$

where R_0 is the box size, which needs to be chosen large enough to make sure the contributions to dynamic dipole polarizabilities from higher excited states are included, especially when the photon energy ω is large. The nonlinear parameter γ also needs to be adjusted to get more accurate ground-state energy of helium, then the value of γ is fixed the same for all the triplet states to simplify the integral of B-splines.

IV. RESULTS AND DISCUSSIONS

In our calculation, $R_0 = 200$ a.u. and $\gamma = 0.038\times R_0$ are used throughout the paper. Using the fixed values of R_0 and γ, the ground-state energy of helium under S-wave approximation with 30 B-splines of order 7 is $-2.879\,028\,4$ a.u., which has seven significant digits with the S-wave limit value $-2.879\,028\,767\,29$ a.u. [35].

A. Energies and oscillator strengths

Table I presents the convergence studies of the energies for the metastable state $2\,^3S$ and the oscillator strengths of $2\,^3S \to 2\,^3P$ transition in the length gauge of helium as the number of basis set and partial waves increased. For the energy, increase of the number of partial wave changed less than the number of B-spline N increased. This convergent style for the energy suggests that we can fix partial wave (in our work we fix $\ell_{\max} = 10$), then increase the number of B-spline N to avoid too enormous a number of CI. Considering both the effect from N and $\ell_{\max}$, the extrapolated values are given in the last line of the Table I. The final converged value for the energy is $-2.175\,229\,36(2)$ a.u., which is in excellent agreement with the result $-2.175\,229\,378\,176$ a.u. of Cann and Thakkar [36]. The extrapolated oscillator strength $0.539\,086\,4(3)$ has six significant digits, compared with the value $0.539\,086\,1$ of Drake [37].

A similar convergence pattern exists for the energies and oscillator strengths in the velocity and acceleration gauges for the other triplet states of helium. The final convergent results of the energies are presented in Table II. Our energies are more accurate than the values [38] by two orders of magnitude, which are obtained by using the B-splines CI method with different number of configuration states, and our results for the $2\,^3S$ and $2\,^3P$ states have eight significant digits, compared with the explicitly correlated calculations [36] and the Hylleraas results [37].

Table III gives a comparison of the oscillator strengths for some selected transitions. For the dipole oscillator strength of the $2\,^3S \to 2\,^3P$ transition, the value in the acceleration gauge is less accurate than the results from length and velocity gauges, but our results for the $2\,^3S \to 2\,^3P$ transition in three

TABLE I. Convergence of the energies (in a.u.) for the metastable state $2\,^3S$ and the oscillator strengths $f^{(L)}_{2^3S\to 2^3P}$ in the length gauge of helium as the number of B-splines N and partial waves $\ell_{\max}$ increased. The numbers in parentheses of the extrapolated values give the computational uncertainties.

	Energy			$f^{(L)}_{2^3S\to 2^3P}$		
$\ell_{\max}$	$N=30$	$N=35$	$N=40$	$N=30$	$N=35$	$N=40$
2	−2.175 220 414 7	−2.175 220 430 6	−2.175 220 434 5	0.539 818 238 0	0.539 818 210 8	0.539 818 205 6
3	−2.175 227 095 0	−2.175 227 116 4	−2.175 227 122 0	0.539 204 607 9	0.539 204 551 9	0.539 204 538 8
4	−2.175 228 582 8	−2.175 228 609 3	−2.175 228 616 5	0.539 117 154 6	0.539 117 068 1	0.539 117 046 0
5	−2.175 229 025 5	−2.175 229 055 9	−2.175 229 064 7	0.539 096 977 2	0.539 096 862 6	0.539 096 831 3
6	−2.175 229 184 7	−2.175 229 218 3	−2.175 229 228 3	0.539 090 770 9	0.539 090 632 7	0.539 090 593 1
7	−2.175 229 250 1	−2.175 229 285 9	−2.175 229 297 0	0.539 088 462 0	0.539 088 305 2	0.539 088 258 3
8	−2.175 229 279 6	−2.175 229 317 1	−2.175 229 328 9	0.539 087 479 3	0.539 087 308 8	0.539 087 255 9
9	−2.175 229 293 9	−2.175 229 332 6	−2.175 229 345 0	0.539 087 017 3	0.539 086 836 5	0.539 086 779 0
10	−2.175 229 301 3	−2.175 229 340 7	−2.175 229 353 6	0.539 086 782 6	0.539 086 594 7	0.539 086 533 6
Extrap.		−2.175 229 36(2)			0.539 086 4(3)	

TABLE II. Comparison of the energies (in a.u.) for the four lowest triplet states of helium. The numbers in the parentheses are the computational uncertainties.

State	Present	Ref. [38]	Ref. [36]	Ref. [37]
$2\,^3S$	−2.175 229 36(2)	−2.175 228 8	−2.175 229 378 176	−2.175 229 378 236 791 30
$3\,^3S$	−2.068 689 07(2)	−2.068 688 8	−2.068 689 067 283	−2.068 689 067 472 457 19
$2\,^3P$	−2.133 164 17(2)	−2.133 163 4	−2.133 164 181 6	−2.133 164 190 779 273(5)
$3\,^3P$	−2.058 081 08(2)	−2.058 080 6	−2.058 081 077 2	−2.058 081 084 274 28(4)

TABLE III. Comparison of the oscillator strengths in three different gauges for helium. The numbers in the parentheses are the computational uncertainties. The values of Ref. [36] are the average of the length and velocity gauges, the results of Ref. [37] are in the length gauge, and Ref. [39] lists the values in three different gauges.

	Present					Ref. [39]		
Transition	$f^{(L)}_{gn}$	$f^{(V)}_{gn}$	$f^{(A)}_{gn}$	Ref. [36]	Ref. [37]	$f^{(L)}_{gn}$	$f^{(V)}_{gn}$	$f^{(A)}_{gn}$
$2\,^3S\to 2\,^3P$	0.539 086 4(3)	0.539 086 5(2)	0.539 078(6)	0.5391	0.539 086 1	0.5392(8)	0.539(3)	0.56(3)
$3\,^3S\to 3\,^3P$	0.890 851 8(2)	0.890 851 8(4)	0.890 83(3)	0.8910	0.890 851 3	0.890(2)	0.889(7)	0.85(6)
$2\,^3P\to 3\,^3D$	0.610 225 5(2)	0.610 225 5(2)	0.610 224 7(3)	0.610 24	0.610 225 2	0.611(2)	0.609(2)	0.609(3)
$2\,^3P\to 2\,^3P^e$	0.180 480 28(2)	0.180 480 3(2)	0.180 480 3(3)					
$3\,^3P\to 4\,^3D$	0.477 594 3(2)	0.477 594 3(2)	0.477 593(3)	0.477 60	0.477 593 8	0.474(3)	0.476(1)	0.494(5)
$3\,^3P\to 3\,^3P^e$	0.135 420 99(2)	0.135 420 99(3)	0.135 420 98(4)					

TABLE IV. Convergence of the static dipole polarizabilities (in a.u.) in three different gauges for the metastable state $2\,^3S$ of helium as the number of B-splines N and partial waves $\ell_{\max}$ increased. The numbers in parentheses give the computational uncertainties.

	$\alpha_1^{(L)}(0)$			$\alpha_1^{(V)}(0)$			$\alpha_1^{(A)}(0)$		
$\ell_{\max}$	$N=30$	$N=35$	$N=40$	$N=30$	$N=35$	$N=40$	$N=30$	$N=35$	$N=40$
2	315.433 490	315.433 397	315.433 373	315.171 086	315.170 980	315.170 949	312.742 586	312.745 210	312.745 924
3	315.606 026	315.605 905	315.605 872	315.571 449	315.571 315	315.571 274	315.072 959	315.076 939	315.078 064
4	315.626 281	315.626 136	315.626 095	315.618 705	315.618 550	315.618 502	315.463 517	315.468 762	315.470 301
5	315.630 187	315.630 024	315.629 976	315.627 938	315.627 769	315.627 715	315.562 445	315.568 761	315.570 684
6	315.631 213	315.631 037	315.630 984	315.630 396	315.630 219	315.630 160	315.594 442	315.601 601	315.603 855
7	315.631 548	315.631 364	315.631 306	315.631 205	315.631 023	315.630 960	315.606 534	315.614 322	315.616 846
8	315.631 678	315.631 487	315.631 426	315.631 515	315.631 330	315.631 265	315.611 603	315.619 840	315.622 577
9	315.631 735	315.631 540	315.631 476	315.631 649	315.631 462	315.631 396	315.613 883	315.622 434	315.625 333
10	315.631 763	315.631 565	315.631 500	315.631 712	315.631 524	315.631 457	315.614 962	315.623 727	315.626 746
Extrap.		315.631 5(2)			315.631 4(2)			315.63(2)	

TABLE V. Comparison of the static dipole polarizabilities (in a.u.) for helium. The numbers in parentheses give the computational uncertainties.

State	$\alpha_1^{(L)}(0)$	$\alpha_1^{(V)}(0)$	$\alpha_1^{(A)}(0)$	Ref. [40]
$2\,^3S$	315.6315(2)	315.6314(2)	315.63(2)	315.631 47(1)
$3\,^3S$	7937.584(2)	7937.583(2)	7937.4(2)	7937.58(1)
$2\,^3P$	46.707 93(4)	46.707 94(4)	46.71(2)	46.707 748 2(3)
$3\,^3P$	17 305.67(3)	17 305.67(4)	17 311(2)	17 305.598(3)

gauges are correspondingly much more accurate than the values in different gauges of Ref. [39] by three orders of magnitude. All of our results in Table III are more accurate than the previous values of Refs. [36,39]. For the oscillator strengths of other transitions, our results in the length and velocity gauges are in excellent agreement with the Hylleraas calculations of Drake [37]. In addition, the oscillator strengths from the initial states $2\,^3P$ and $3\,^3P$ transit to the unnatural parity states $2\,^3P^e$ and $3\,^3P^e$ are also listed in the Table III.

B. Static dipole polarizabilities

Table IV gives the convergence of the static dipole polarizabilities for the metastable state $2\,^3S$ of helium as the number of basis set and partial waves increased, and the last line lists the extrapolated values. From this table, we can see in the length and velocity gauges that the convergence style is the same, and the results are decreased as the number of basis sets N increased for the same $\ell_{\max}$. However in the acceleration gauge, the values are increased as the number of basis sets N increased for the same $\ell_{\max}$. The final convergent value in the length gauge is 315.631 5(2), which has six significant digits compared with the most accurate Hylleraas value 315.631 47(1) of Yan [40].

Table V presents a comparison of static dipole polarizabilities for the four lowest triplet states of helium. The results between the length and velocity gauges are in good agreement. The values obtained in the acceleration gauge are less accurate than the results in the length and velocity gauges by two orders of magnitude. Present results for the $2\,^3S$ and $3\,^3S$ states in the length and velocity gauges agree with the Hylleraas values [40] at the 10^{-7} level of accuracy, and our values for the $2\,^3P$ and $3\,^3P$ states in the length and velocity gauges agree with the Hylleraas values [40] at the 10^{-6} level of accuracy. In the acceleration gauge, present $\alpha_1^{(A)}(0)$ for $2\,^3P$ and $3\,^3P$ states just have three significant digits compared with the Hylleraas values of Ref. [40].

C. Dynamic dipole polarizabilities

Table VI lists the dynamic dipole polarizability for the metastable state $2\,^3S$ of helium for some selective photon energy from 0 to 0.12 a.u.; the figures in parentheses represent computational uncertainties. It is seen from this table that all of our values have at least five significant digits except the results of $\omega = 0.04$ a.u., $\omega = 0.110$ a.u., and $\omega = 0.115$ a.u., which have four significant digits.

TABLE VI. Comparison of the dynamic dipole polarizabilities (in a.u.) of the $2\,^3S$ state for the He atom. The numbers in parentheses give the computational uncertainties.

ω	Present	Ref. [27]	Ref. [28]	Ref. [31]	Ref. [32]
0.000	315.6315(2)	(315.61, 316.83)	315.63	315.630	315.92
0.005	320.0105(2)	(319.99, 321.23)	320.01	320.009	320.31
0.010	333.9323(2)	(333.91, 335.21)	333.93	333.931	334.25
0.015	360.1322(2)	(360.10, 361.53)	360.12	360.130	360.50
0.020	404.8286(2)	(404.79, 406.43)	404.81	404.825	405.28
0.025	482.3411(3)	(482.29, 484.29)	482.31	482.335	482.95
0.030	631.4758(3)	(631.39, 634.10)	631.42	631.463	632.41
0.035	1001.751(2)	(1001.53, 1006.08)	1001.59	1001.71	1003.68
0.040	3192.7(2)	(3190.16, 3207.18)	3190.67	3192.17	3205.28
0.045	−2097.602(3)	(−14 717.51, −2050.70)	−2098.66	−2097.89	−2097.0
0.050	−725.4477(2)	(−729.45, −718.73)	−725.60	−727.490	−726.27
0.055	−416.4749(2)	(−419.07, −413.67)	−416.54	−416.492	−417.20
0.060	−281.127 19(2)	(−283.14, −279.41)	−281.16	−281.137	−281.78
0.065	−205.599 18(2)	(−207.31, −204.30)	−205.63	−205.606	−206.21
0.070	−157.5702(2)	(−159.14, −156.44)	−157.59	−157.575	−158.17
0.075	−124.336 28(2)	(−125.87, −123.25)	−124.35	−124.340	−124.94
0.080	−99.863 44(2)	(−101.47, −98.72)	−99.88	−99.867	−100.49
0.085	−80.8752(2)	(−82.67, −79.60)	−80.89	−80.878	−81.55
0.090	−65.363 52(2)	(−67.54, −63.84)	−65.37	−65.366	−66.11
0.095	−51.884 20(2)	(−54.81, −49.93)	−51.92	−51.888	−52.74
0.100	−39.052 27(2)	(−43.49, −36.31)	−39.11	−39.059	−40.07
0.105	−24.690 53(2)	(−32.65, −20.33)	−24.82	−24.709	−26.03
0.110	−2.1515(2)		−2.66	−2.248	
0.115	93.381(2)	(−6.27, 128.35)	84.66	91.175	74.32
0.120	−125.6637(4)		−137.94		

TABLE VII. Convergence of the dynamic dipole polarizabilities (in a.u.) for some selective photon energy ω for the metastable state $2\,^3S$ of helium as the box size R_0 increased. The numbers of B-splines and partial waves are set as $N = 40$ and $\ell_{\max} = 10$ respectively.

R_0	$\omega = 0.020$	$\omega = 0.110$	$\omega = 0.140$	$\omega = 0.160$	$\omega = 0.164$
50	404.828 532 675	−2.151 541 215	1.645 391 572	−45.869 633 168	−26.113 507 642
100	404.828 556 614	−2.151 521 839	1.909 710 113	−5.056 386 587	−17.496 811 920
200	404.828 586 773	−2.151 507 768	1.909 749 852	−4.663 840 402	−10.341 706 169
300	404.828 617 985	−2.151 493 277	1.909 789 064	−4.663 839 680	−10.341 970 925
Extrap.	404.8286(2)	−2.1515(2)	1.9098(1)	−4.6638(2)	−10.342(1)

Table VI also makes a comparison of the present results with available values from other literatures [28,31,32]. All of ours results lie within the boundary of Glover and Weinhold's [27], which gives the rigorous upper and lower limits for the dynamic dipole polarizability at a wide photon energy range. In the low photon energy region, our values are in good agreement with Ref. [31], which are also obtained by using the B-spline CI method. For example, our values have the five significant digits compared with theirs. As the photon energy ω increased, the differences between present results and values of Ref. [31] increased; especially for $\omega = 0.115$ a.u., the difference of the dynamic polarizabilities can reach about $2.2a_0^3$. The reason for this is the results for large ω depend on the choice of the box size R_0 of the B-spline. As ω increased, R_0 should be chosen big enough to make sure the transition to high-excited states, especially the transition energies of those excited states near ω, can be included in the calculation of polarizabilities.

It is seen from the Table VII, which presents a convergence study of the dynamic dipole polarizability of helium in the metastable state $2\,^3S$ for some selective ω as the box size R_0 increased, that the numbers of B-splines and partial waves are set as $N = 40$ and $\ell_{\max} = 10$ respectively. The convergence pattern shows that when the photon energy ω is small, the dynamic dipole polarizability can converge very well under small box size. Taking $\omega = 0.020$ a.u. and $\omega = 0.110$ a.u. for examples, the dynamic dipole polarizabilities under $R_0 = 50$ a.u. have six and five significant digits. But for the larger photon energies of $\omega = 0.140$ a.u. and $\omega = 0.160$ a.u., if the box size $R_0 = 200$ a.u. is adopted, the values are $\alpha_1(0.140) = 1.909\,749\,852a_0^3$ and $\alpha_1(0.160) = -4.663\,840\,402a_0^3$. If the box size is set as $R_0 = 50$ a.u., then the values are $\alpha_1(0.140) = 1.645\,391\,572a_0^3$ and $\alpha_1(0.160) = -45.869\,633\,168a_0^3$, which are not convergent compared with their extrapolated values of $\alpha_1(0.140) = 1.9098(1)a_0^3$ and $\alpha_1(0.160) = -4.6638(2)a_0^3$. However, the box size is not the bigger the better for the B-spline CI calculation; oppositely, the loss of accuracy will occur under the same number of B-spline for the big box size. This can be seen from the values of $\omega = 0.160$ a.u. and $\omega = 0.164$ a.u. The dynamic dipole polarizabilities under the $R_0 = 300$ a.u. are not better than the values under $R_0 = 200$ a.u. So in order to get more accurate values, the number of B-spline should be increased, which makes the number of CI

TABLE VIII. Dynamic polarizabilities (in a.u.) of $3\,^3S$, $2\,^3P$, and $3\,^3P$ states for the He atom. The numbers in parentheses give the computational uncertainties.

State	$3\,^3S$	$2\,^3P$		$3\,^3P$	
ω	$\alpha_1(\omega)$	$\alpha_1(\omega)$	$\alpha_1^T(\omega)$	$\alpha_1(\omega)$	$\alpha_1^T(\omega)$
0.000	7937.584(2)	46.707 93(3)	69.5964(2)	17 305.67(3)	336.768(3)
0.005	10 199.363(2)	45.832 74(4)	70.8984(2)	−8051.87(2)	3534.464(2)
0.010	71 124.62(5)	42.976 03(4)	75.0559(2)	−23 498.47(2)	23 293.67(2)
0.015	−7892.735(2)	37.3217(2)	82.9492(2)	3942.877(2)	−3345.9627(4)
0.020	−3062.782(2)	26.972(2)	96.591 95(3)	4749.082(4)	−3445.013(2)
0.025	−1685.264(2)	7.4367(2)	120.658 74(3)	4962.08(2)	−246.35(2)
0.030	−1031.851(2)	−33.776 38(2)	167.923 35(6)	−2249.18(2)	111.731(2)
0.035	−305.1046(2)	−145.8045(2)	287.9533(2)	502.52(2)	−765.454(5)
0.040	−792.8559(2)	−860.666(3)	1013.44(2)	−1078.384(2)	53.0407(4)
0.045	−512.4321(2)	924.3286(4)	−757.2164(4)	−1078.7(2)	78.96(2)
0.050	−602.5701(5)	498.7080(2)	−311.6507(2)	152(2)	14.1(2)
0.055	−703.68(2)	447.8331(3)	−231.6643(2)		
0.060	−620.32(3)	517.4623(6)	−255.4211(4)		
0.065		−563.39(2)	907.7(2)		
0.070		561.824(2)	−27.2995(3)		
0.075		1635.892(8)	−167.107(2)		
0.080		−1497.409(7)	137.702(2)		
0.085		−418.409(2)	26.1352(2)		
0.090		−185.5369(3)	−1.0091(2)		
0.095		−29.424(2)	−39.1638(3)		
0.100		211.866(3)	−18.9742(3)		

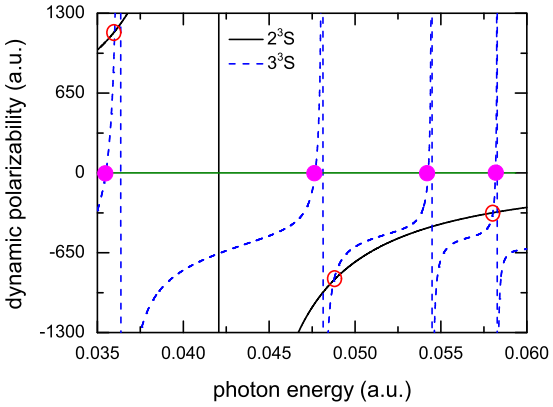

FIG. 1. (Color online) Dynamic dipole polarizabilities (in a.u.) of helium for the photon energy $0.035 \leqslant \omega \leqslant 0.06$ a.u. The solid black line denotes the dynamic polarizabilities for $2\,^3S$ state, and the dashed blue line represents the dynamic polarizabilities for $3\,^3S$ state. The crossing points denoted as solid magenta circle are the tune-out wavelengths, and the crossing points marked as blank red circle are the magic wavelengths. The vertical lines are the resonance transition positions, and the green line is a horizontal zero line.

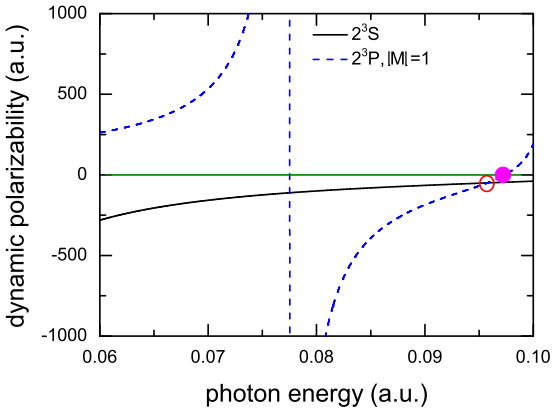

FIG. 3. (Color online) Dynamic dipole polarizabilities (in a.u.) of helium for the photon energy $0.06 \leqslant \omega \leqslant 0.10$ a.u. The solid black line denotes the dynamic polarizabilities for $2\,^3S$ state, and the dashed blue line represents the dynamic polarizabilities for $2\,^3P(|M| = 1)$ state. The crossing points denoted as solid magenta circle are the tune-out wavelengths, and the crossing points marked as blank red circle are the magic wavelengths. The vertical lines are the resonance transition positions, and the green line is a horizontal zero line.

increased exponentially and slows down the convergent rate of our calculations. So in our practical calculations, we need to choose appropriate R_0 to get accurate values for large ω and to avoid a large number of CI at the same time.

Table VIII lists some selective values of dynamic dipole polarizabilities of $2\,^3P$, $3\,^3S$, and $3\,^3P$ states for the He atom. For the $2\,^3P$ state, the dynamic dipole polarizabilities for ω below the second excitation threshold are listed, and for the $3\,^3S$ and $3\,^3P$ states, the dynamic dipole polarizabilities for ω below the first ionization threshold are obtained. All of our results are very accurate except a few values for the photon energy ω near resonance transition energy or ionization threshold.

The dynamic dipole polarizabilities for the lowest four triplet states of helium are also plotted in the Figs. 1–6 as the photon energy ω. For the nonzero angular momentum state, the polarizability depends upon its magnetic quantum number M because of both scalar and tensor polarizabilities existing, so the dynamic dipole polarizabilities for $2\,^3P$ and $3\,^3P$ states are divided into two cases as $M = 0$ and $|M| = 1$. The crossing points between a curve and the horizontal zero line are labeled as tune-out wavelengths, denoted as a solid magenta circle, and the crossing points between two curves are the magic wavelengths, denoted as a blank red circle. The vertical lines are the resonance transition positions.

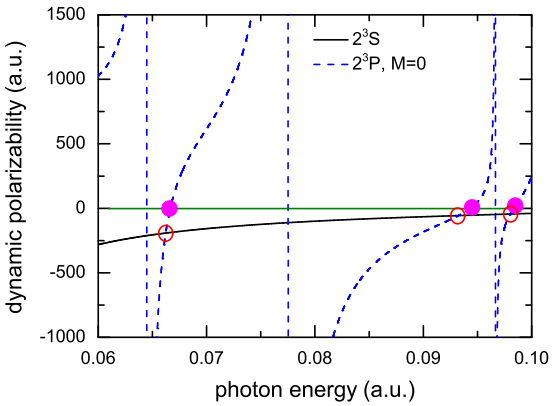

FIG. 2. (Color online) Dynamic dipole polarizabilities (in a.u.) of helium for the photon energy $0.06 \leqslant \omega \leqslant 0.10$ a.u. The solid black line denotes the dynamic polarizabilities for $2\,^3S$ state, and the dashed blue line represents the dynamic polarizabilities for $2\,^3P(M = 0)$ state. The crossing points denoted as solid magenta circle are the tune-out wavelengths, and the crossing points marked as blank red circle are the magic wavelengths. The vertical lines are the resonance transition positions, and the green line is a horizontal zero line.

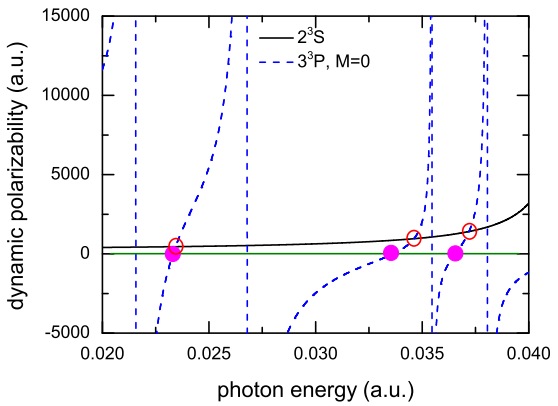

FIG. 4. (Color online) Dynamic dipole polarizabilities (in a.u.) of helium for the photon energy $0.02 \leqslant \omega \leqslant 0.04$ a.u. The solid black line denotes the dynamic polarizabilities for $2\,^3S$ state, and the dashed blue line represents the dynamic polarizabilities for $3\,^3P(M = 0)$ state. The crossing points denoted as solid magenta circle are the tune-out wavelengths, and the crossing points marked as blank red circle are the magic wavelengths. The vertical lines are the resonance transition positions, and the green line is a horizontal zero line.

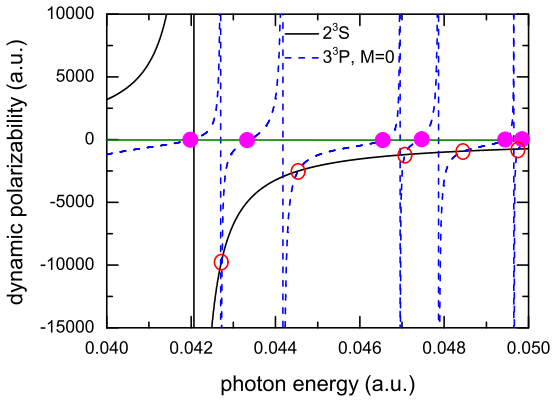

FIG. 5. (Color online) Dynamic dipole polarizabilities (in a.u.) of helium for the photon energy $0.04 \leqslant \omega \leqslant 0.05$ a.u. The solid black line denotes the dynamic polarizabilities for $2\,^3S$ state, and the dashed blue line represents the dynamic polarizabilities for $3\,^3P(M=0)$ state. The crossing points denoted as solid magenta circle are the tune-out wavelengths, and the crossing points marked as blank red circle are the magic wavelengths. The vertical lines are the resonance transition positions, and the green line is a horizontal zero line.

D. Tune-out wavelengths

Table IX lists the values of tune-out wavelengths in the 400–4200-nm region, marked as a solid magenta circle in Figs. 1–6. For the metastable state of helium, Mitroy and Tang [4] have obtained the tune-out wavelength of 413.02(9) nm by incorporating Hylleraas matrix elements for the transition to $2\,^3P$ and $3\,^3P$ manifolds and core-polarization model matrix elements for other transitions, and they predicted that the tune-out wavelength around 413 nm can be used to test the QED effect. Recently, an experimental measurement of Ken Baldwin's group reports the tune-out wavelength being 413.0938(9 Stat.)(20 Syst.) nm [5] and another theoretical calculation by Notermans *et al.* [7] gives the

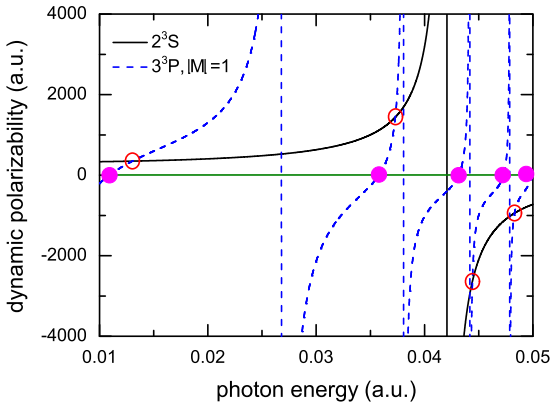

FIG. 6. (Color online) Dynamic dipole polarizabilities (in a.u.) of helium for the photon energy $0.01 \leqslant \omega \leqslant 0.05$ a.u. The solid black line denotes the dynamic polarizabilities for $2\,^3S$ state, and the dashed blue line represents the dynamic polarizabilities for $3\,^3P(|M|=1)$ state. The crossing points denoted as solid magenta circle are the tune-out wavelengths, and the crossing points marked as blank red circle are the magic wavelengths. The vertical lines are the resonance transition positions, and the green line is a horizontal zero line.

TABLE IX. Tune-out wavelengths (λ_t) for $2\,^3S$, $3\,^3S$, $2\,^3P$, and $3\,^3P$ states of helium. The second and third columns are the tune-out wavelengths in atomic units and nanometer respectively. The numbers in parentheses give the computational uncertainties.

State	ω_t (a.u.)	λ_t (nm)
$2\,^3S$	**0.110 312 66(2)**	**413.038 28(3)**
$3\,^3S$	0.035 488 102(2)	1283.905 03(4)
	0.047 681 245(3)	955.582 28(7)
	0.054 260 56(3)	839.714(2)
	0.058 175 6(2)	783.204(2)
$2\,^3P(M=0)$	0.066 652 71(2)	683.5934(2)
	0.094 341 03(2)	482.9644(2)
	0.098 338 54(2)	463.3316(2)
$2\,^3P(M=\pm1)$	0.097 382 82(2)	467.8788(2)
$3\,^3P(M=0)$	0.023 315 997(3)	1954.1670(3)
	0.033 637 088(2)	1354.5570(2)
	0.036 548 517(2)	1246.6539(3)
	0.042 005 02(2)	1084.712(2)
	0.043 390 63(3)	1050.074(2)
	0.046 593 9(2)	977.883(2)
	0.047 403 1(2)	961.189(3)
	0.049 442 7(2)	921.539(4)
	0.049 964 4(2)	911.917(4)
$3\,^3P(M=\pm1)$	0.010 911 33(2)	4175.783(4)
	0.035 787 67(2)	1273.1580(2)
	0.043 149 27(2)	1055.9472(3)
	0.047 294 5(1)	963.397(2)
	0.049 905 4(1)	912.995(3)

tune-out wavelength of 414.197 nm by using available tables of level energies and Einstein A coefficients. Our tune-out wavelength of *ab initio* calculation is 413.038 28(3) nm, which corroborates the value 413.02(9) nm of Mitroy and Tang [4]. The difference between the theoretical calculations and the experimental measurement may be caused by finite nuclear mass, relativistic, and QED corrections, which calls for great efforts of theoretical calculation to improve the precision for the QED test.

E. Magic wavelengths

The magic wavelength is the wavelength at which the polarizability difference for a transition goes to zero, which means the first-order Stark shifts for the upper and lower levels of a transition are the same [41,42]. Table X presents all the values of magic wavelengths in the 460–3500-nm region marked in the blank red circle in Figs. 1–6. The corresponding dynamic dipole polarizabilities at the magic wavelengths are also given in the last column. For the magic wavelength of 1066.197(2) nm, there exist two terms, which play a major contribution of the dynamic dipole polarizabilities for the $2\,^3S$ and $3\,^3P(M=0)$ states respectively. Table XI lists some contributions from different intermediate states for the $2\,^3S \rightarrow 3\,^3P(M=0)$ transition at the magic wavelength of 1066.197(2) nm. We can see that the contribution from the $2\,^3P$ state to the polarizability of $2\,^3S$ is about 99.87%, and the contribution from the $6\,^3S$ state to the polarizability of $3\,^3P(M=0)$ is about 98.87%. According to the definition

TABLE X. Magic wavelengths (λ_m) for $2\,^3S \to 3\,^3S$, $2\,^3S \to 2\,^3P(M=0,\pm1)$, and $2\,^3S \to 3\,^3P(M=0,\pm1)$ transitions of the He atom. The corresponding dynamic dipole polarizabilities at the magic wavelengths are given in the last column. The numbers in parentheses give the computational uncertainties.

Transition	ω_m (a.u.)	λ_m (nm)	$\alpha_1(\omega_m)$ (a.u.)
$2\,^3S \to 3\,^3S$	0.036 004 592(2)	1265.487 24(4)	1151.058(2)
	0.048 775 162(5)	934.1507(2)	−872.007(2)
	0.058 024 4(2)	785.245(3)	−324.31(2)
$2\,^3S \to 2\,^3P(M=0)$	0.066 228 54(2)	687.9716(2)	−191.9157(2)
	0.093 229 5(2)	488.7225(2)	−56.5068(2)
	0.098 016 6(2)	464.8532(3)	−44.169 53(4)
$2\,^3S \to 2\,^3P(M=\pm1)$	0.095 747 3(2)	475.870 85(6)	−49.962 90(4)
$2\,^3S \to 3\,^3P(M=0)$	0.023 434 415(3)	1944.2923(3)	453.0297(2)
	0.034 618 094(3)	1316.1716(2)	955.639(2)
	0.037 202 637 7(2)	1224.734 46(2)	1410.365(2)
	0.042 734 44(3)	**1066.197(2)**	−9487(2)
	0.044 532 37(2)	1023.151(2)	−2511.07(3)
	0.047 069 3(2)	968.007(3)	−1196.32(3)
	0.048 478 5(2)	939.867(4)	−915.97(3)
	0.049 762 5(3)	915.616(5)	−750.19(3)
$2\,^3S \to 3\,^3P(M=\pm1)$	0.013 031 86(2)	3496.304(3)	348.0648(2)
	0.037 297 86(2)	1221.607 75(2)	1436.592(2)
	0.044 421 15(2)	1025.713(2)	−2633.59(3)
	0.048 309 5(2)	943.156(4)	−942.89(2)

of magic wavelength $\alpha_{2^3S}(\omega_m) = \alpha_{3^3P}(\omega_m)$, we have the expanded form,

$$\frac{f_{2^3S\to2^3P}}{\Delta E^2_{2^3S\to2^3P} - \omega_m^2} + \alpha_{2^3S}(\text{Remainder};\omega_m) = \frac{3f_{3^3P\to6^3S}}{\Delta E^2_{3^3P\to6^3S} - \omega_m^2} + \alpha_{3^3P}(\text{Remainder};\omega_m), \quad (25)$$

where the second term in the left of Eq. (25) is all the contributions from other $n\,^3P$ states to the dynamic dipole polarizability of $2\,^3S$ state, and the second term in the right of Eq. (25) is all the contributions from other $n\,^3S$, $n\,^3D$, and $n\,^3P^e$ states to the dynamic dipole polarizability of the $3\,^3P(M=0)$ state. If all the remainder terms are neglected, then the ratios of oscillator strengths and reduced matrix elements are written as

$$\frac{f_{2^3S\to2^3P}}{f_{3^3P\to6^3S}} = \frac{3\left(\Delta E^2_{2^3S\to2^3P} - \omega_m^2\right)}{\Delta E^2_{3^3P\to6^3S} - \omega_m^2}, \quad (26)$$

$$\frac{M_{2^3S\to2^3P}}{M_{3^3P\to6^3S}} = \frac{\left|\left\langle 2\,^3S\right\| \sum_{i=1,2} r_i C^{(1)}(\hat{r}_i) \left\|2\,^3P\right\rangle\right|}{\left|\left\langle 3\,^3P\right\| \sum_{i=1,2} r_i C^{(1)}(\hat{r}_i) \left\|6\,^3S\right\rangle\right|} = \sqrt{\frac{\Delta E_{3^3P\to6^3S}\left(\Delta E^2_{2^3S\to2^3P} - \omega_m^2\right)}{\Delta E_{2^3S\to2^3P}\left(\Delta E^2_{3^3P\to6^3S} - \omega_m^2\right)}}. \quad (27)$$

TABLE XI. Contributions from some intermediate states to the dynamic dipole polarizability of $2\,^3S$ and $3\,^3P(M=0)$ states at the magic wavelengths 1066.197(2) nm.

ω (a.u.)	0.042 734 44(3)
λ (nm)	1066.197(2)
Intermediate states	$2\,^3S$
$2\,^3P$	**−9499.066**
$3\,^3P$	5.418
$4\,^3P$	1.386
Others	5.234
Total	**−9487.028**
Intermediate states	$3\,^3P\ (M=0)$
$3\,^3S$	519.840
$4\,^3S$	−320.109
$5\,^3S$	−118.888
$6\,^3S$	**−9379.600**
$3\,^3D$	−73.9017
$4\,^3D$	−517.059
$5\,^3D$	−395.758
$6\,^3D$	506.415
Others	292.0327
Total	**−9487.028**

Combined present energy difference and the magic wavelength 1066.197(2) nm, the ratios of the oscillator strengths, and the reduced matrix elements are determined and listed in Table XII. "Present[1]" are the values of our *ab initio* calculation,

TABLE XII. Comparison of the ratios for the oscillator strengths $(f_{2^3S\to2^3P})/(f_{3^3P\to6^3S})$ and the reduced matrix elements $(M_{2^3S\to2^3P})/(M_{3^3P\to6^3S})$. Present[1] are the value of our *ab initio* calculation, and Present[2] are derived by substituting our theoretical energies and the magic wavelength of 1066.197(2) nm into Eqs. (26) and (27). The numbers in parentheses give the computational uncertainties.

	$(f_{2^3S\to2^3P})/(f_{3^3P\to6^3S})$	$(M_{2^3S\to2^3P})/(M_{3^3P\to6^3S})$
Present[1]	65.48(2)	4.7073(3)
Present[2]	64.6653	4.677 847
Ref. [36]	65.5308	4.789 739

and "Present[2]" are derived by substituting our theoretical energies and the magic wavelength of 1066.197(2) nm into Eqs. (26) and (27). Compared with the explicitly correlated results of Ref. [36], it can be believed that the values of "Present[1]" are reliable, since present oscillator strengths for $2\,^3S \to 2\,^3P$ and $3\,^3P \to 6\,^3S$ transitions are much more accurate than the values of Ref. [36] by at least one order of magnitude. In order to test the accuracy of the values derived from Eqs. (26) and (27), we can compare the results between Present[1] and Present[2]. It is clearly seen that the derived values 64.6653 and 4.677 847 from Eqs. (26) and (27) are in good agreement with our *ab initio* values 65.48(2) and 4.7073(3) at the level of 1.3% and 0.7% accuracy respectively. If one increases the number of B-spline basis sets, and also considers the contribution of the remainder term, then improvement of the accuracy for the ratio of two transition matrix elements $(M_{2\,^3S\to 2\,^3P})/(M_{3\,^3P\to 6\,^3S})$ up to 0.5% is achievable.

Currently, however, present experimental technique is very difficult to measure matrix elements accurately; only 1% accuracy for one or two of the lowest transitions has been reported [43,44]. Recently, Herold *et al.* presented a method for accurate determination of $5s - 6p$ matrix elements in rubidium by measurements of the ac Stark shift around tune-out wavelength [3]. In our calculation, the particular magic wavelength around 1066 nm can be used for experiment measurement to determine the atomic transition matrix elements involved in highly excited states for helium.

V. CONCLUSIONS

The calculations of the energies and the main oscillator strengths for the four triplet states ($2\,^3S$, $3\,^3S$, $2\,^3P$, and $3\,^3P$) in the length, velocity, and acceleration gauges are carried out by the configuration interaction based on the B-spline functions. Also the accurate dynamic dipole polarizabilities for the four lowest triplet states are obtained. Our static dipole polarizabilities in the length and velocity gauges have five to six significant digits, which are in excellent agreement with the variational Hylleraas calculations. The present work lays a solid foundation to further calculate the relativistic and QED effects on the dynamic polarizabilities of helium.

In particular, the tune-out wavelengths for the four triplet states and magic wavelengths for the three transitions of $2\,^3S \to 3\,^3S$, $2\,^3S \to 2\,^3P$, and $2\,^3S \to 3\,^3P$ are determined with high precision. Our tune-out wavelength 413.038 28(3) nm of the metastable state validates the value of Mitroy and Tang [4]. And the magic wavelength around 1066 nm for the $2\,^3S \to 3\,^3P$ transition is proposed for experimental measurement to determine the ratio of the transition matrix elements $(2\,^3S \to 2\,^3P)/(3\,^3P \to 6\,^3S)$; this is a unique way to obtain an accurate transition matrix element involved in highly excited states. Also we expect that other tune-out wavelengths and magic wavelengths can provide theoretical references for the precision-measurement experiment design in the future.

ACKNOWLEDGMENTS

We acknowledge many insightful discussions with the late James Mitroy. We also thank Dr. C.-B. Li for carefully reading this manuscript. This work was supported by the National Basic Research Program of China under Grant No. 2012CB821305 and by the National Natural Science Foundation of China under Grants No. 11474319 and No.11274348.

[1] J. Mitroy, M. S. Safronova, and C. W. Clark, J. Phys. B **43**, 202001 (2010).
[2] Y.-B. Tang, H.-X. Qiao, T.-Y. Shi, and J. Mitroy, Phys. Rev. A **87**, 042517 (2013).
[3] C. D. Herold, V. D. Vaidya, X. Li, S. L. Rolston, J. V. Porto, and M. S. Safronova, Phys. Rev. Lett. **109**, 243003 (2012).
[4] J. Mitroy and L.-Y. Tang, Phys. Rev. A **88**, 052515 (2013).
[5] B. M. Henson, R. I. Khakimov, R. G. Dall, K. G. H. Baldwin, L.-Y. Tang, and A. G. Truscott, arXiv:1505.03642.
[6] M. S. Safronova, U. I. Safronova, and C. W. Clark, Phys. Rev. A **86**, 042505 (2012).
[7] R. P. M. J. W. Notermans, R. J. Rengelink, K. A. H. van Leeuwen, and W. Vassen, Phys. Rev. A **90**, 052508 (2014).
[8] G. W. F. Drake and Z. C. Yan, Can. J. Phys. **86**, 45 (2008).
[9] E. E. Eyler, D. E. Chieda, M. C. Stowe, M. J. Thorpe, T. R. Schibli, and J. Ye, Eur. Phys. J. D **48**, 43 (2008).
[10] M. L. Lewis and P. H. Serafino, Phys. Rev. A **18**, 867 (1978).
[11] K. Pachucki and V. A. Yerokhin, Phys. Rev. Lett. **104**, 070403 (2010).
[12] M. Smiciklas and D. Shiner, Phys. Rev. Lett. **105**, 123001 (2010).
[13] R. van Rooij, J. S. Borbely, J. Simonet, M. D. Hoogerland, K. S. E. Eikema, R. A. Rozendaal, and W. Vassen, Science **333**, 196 (2011).
[14] P. Cancio Pastor, L. Consolino, G. Giusfredi, P. De Natale, M. Inguscio, V. A. Yerokhin, and K. Pachucki, Phys. Rev. Lett. **108**, 143001 (2012).
[15] V. A. Yerokhin and K. Pachucki, Phys. Rev. A **81**, 022507 (2010).
[16] H. Schomerus1, Y. Noat, J. Dalibard, and C. W. J. Beenakker, Europhys. Lett. **76**, 409 (2006).
[17] A. S. Tychkov, J. C. J. Koelemeij, T. Jeltes, W. Hogervorst, and W. Vassen, Phys. Rev. A **69**, 055401 (2004).
[18] G. W. F. Drake, Phys. Scr. **T83**, 83 (1999).
[19] G. W. F. Drake, Phys. Scr. **T95**, 22 (2001).
[20] G. W. F. Drake, M. M. Cassar, and R. A. Nistor, Phys. Rev. A **65**, 054501 (2002).
[21] L.-Y. Tang, Y.-B. Tang, T.-Y. Shi, and J. Mitroy, J. Chem. Phys. **139**, 134112 (2013).
[22] M. J. Jamieson, G. W. F. Drake, and A. Dalgarno, Phys. Rev. A **51**, 3358 (1995).
[23] M. Masili and A. F. Starace, Phys. Rev. A **68**, 012508 (2003).
[24] S. Kar, Phys. Rev. A **86**, 062516 (2012).
[25] C. Schwartz, arXiv:math-ph/0605018.
[26] K. Pachucki and J. Sapirstein, Phys. Rev. A **63**, 012504 (2000).
[27] R. M. Glover and F. Weinhold, J. Chem. Phys. **66**, 185 (1977).
[28] K. T. Chung, Phys. Rev. A **15**, 1347 (1977).
[29] C. de. Boor, *A Practical Guide to Splines* (Springer, New York, 1978).

[30] M. K. Chen, J. Phys. B **28**, 1349 (1995).
[31] M. K. Chen, J. Phys. B **28**, 4189 (1995).
[32] M. Rérat, M. Caffarel, and C. Pouchan, Phys. Rev. A **48**, 161 (1993).
[33] V. E. Chernov, D. L. Dorofeev, I. Y. Kretinin, and B. A. Zon, J. Phys. B **38**, 2289 (2005).
[34] M. Rérat and C. Pouchan, Phys. Rev. A **49**, 829 (1994).
[35] P. Decleva, A. Lisini, and M. Venuti, Int. J. Quantum Chem. **56**, 27 (1995).
[36] N. M. Cann and A. J. Thakkar, Phys. Rev. A **46**, 5397 (1992).
[37] G. W. F. Drake, *Handbook of Atomic, Molecular and Optical Physics* (American Institute of Physics, New York, 1996).
[38] M. K. Chen, J. Phys. B **27**, 865 (1994).
[39] S. A. Alexander and R. L. Coldwell, J. Chem. Phys. **124**, 054104 (2006).
[40] Z. C. Yan, Phys. Rev. A **62**, 052502 (2000).
[41] J. Ye, D. W. Vernooy, and H. J. Kimble, Phys. Rev. Lett. **83**, 4987 (1999).
[42] M. S. Safronova, U. I. Safronova, and C. W. Clark, Phys. Rev. A **87**, 052504 (2013).
[43] E. Gomez, S. Aubin, L. A. Orozco, and G. D. Sprouse, J. Opt. Soc. Am. B **21**, 2058 (2004).
[44] N. Bouloufa, A. Crubellier, and O. Dulieu, Phys. Scr. **T134**, 014014 (2009).